Journal of Engineering Sciences, Assiut University, Vol. 40, No. 4, pp.1055 -1074, July 2012

STEPWISE EROSION AS A METHOD FOR INVESTIGATING THE WEAR MECHANISMS AT DIFFERENT IMPACT ANGLES IN SLURRY EROSION

Y. M. Abd-Elrhman[1], A. Abouel-Kasem[2], S. M. Ahmed[3], and K.M. Emara[4]

[1]Mechanical Engineering Department, Faculty of Engineering, Assiut University, Assiut71516, Egypt, E-mails: y_mahmoud_a@hotmail.com
[2] Mechanical Engineering Department, Faculty of Eng.-Rabigh, King Abdulaziz University, P.O. Box 344, Rabigh 21911, Saudi Arabia; Department of Mechanical Engineering, Assiut University, Assiut 71516, Egypt, E-mails: abouelkasem@yahoo.com
[3]Mechanical Engineering Department, Faculty of Engineering, Majmaah University ,Saudi Arabia, E-mails: shemy2007@yahoo.com
[4]Mechanical Engineering Department, Faculty of Engineering, Assiut University, Assiut71516, Egypt, E-mails: emara@aun.edu.eg

(Received April 7, 2012 Accepted May 13, 2012)

In the present work, stepwise erosion technique was carried out to investigate in detail the influence of impact angle on the erosion process of AISI 5117 steel. The impact sites number and their morphology at different impact angles were investigated using SEM examination and image analysis. In addition, the SEM images of eroded surface using stepwise technique were used presented for better understanding of material removal at different angles. The tests were carried out with particle concentration of 1 wt %, and the impact velocity of slurry stream was 15 m/s. Silica sand has a nominal size range of 250 – 355 μm was used as an erodent, using whirling-arm test rig. The results showed that the number of craters as expected increases with the increase in the mass of erodent for all impact angles and that this number decreases with the increase of the impact angle. In addition, the counted number of craters is larger than the calculated number of particles for all impact angles and at any stage. The effect of impact angle based on the impact crater shape can be divided into two regions; the first region for $\theta \leq 60o$ and the second region for $\theta \geq 75o$. In the first region the length of the tracks decreases with the increase of impact angle. The calculated size ranges from few micrometers to 100 micrometer for the first region and to 50 micrometers in the second region. Chipping of the former impact sites by subsequent impact particles plays important role in developing erosion.

KEYWORDS: *Slurry erosion, Impact angle, Number of impact sites, Eroded surface, Erosion mechanisms, AISI 5117steel, Particles rebound effect.*

1. INTRODUCTION

Erosion wear is a process of progressive removal of material from a target surface due to repeated impacts of solid particles. The particles suspended in the flow of solid–

liquid mixture erode the wetted passages limiting the service life of equipment used in many industrial applications such as: oil field mechanical equipment, solid-liquid hydro transportation systems, hydroelectric power station, coal liquefaction plants and industrial boilers where coal is carried directly as a fuel in water or oil as reported in Refs. [1-6].

Slurry erosion (solid-liquid erosion) is a complex phenomenon and it is not yet fully understood because it is influenced by many factors, which act simultaneously. These factors include flow field parameters, target material properties and erodent particle characteristics. Among these parameters, the impact angle and microstructure of the target material play an important role in the material removal process, based on the data reported in Refs. [7-11]. Materials are characterized as either ductile or brittle according to dependence of their erosion rate on the angle of attack curves [7-9]. For ductile material the erosion rate increases from zero at 0^o impact angle to a maximum when the angle of impact is increased to between 30^o and 50^o. After reaching the maximum, the erosion rate decreases to a minimum value at 90^o. The effect of impact angle erosion mechanisms of 1017 steel and high-Cr white cast iron using a slurry whirling-arm test rig were carried out by the authors [12]. Test results showed that, the effect of impact angle on erosion mechanisms of 1017 steel has three regions. In the first region ($\theta \leq 15^o$) shallow ploughing and particle rolling were the dominant erosion mechanisms, microcutting and deep ploughing in the second region ($15^o < \theta < 75^o$), while indentations and material extrusion prevailed in the third region ($\theta \geq 75^o$). For high-Cr white cast iron the test results showed that, the erosion mechanisms involved both plastic deformation of the ductile matrix and brittle fracture of the carbides. At low impact angles (up to 45^o) observations of microphotographs of the impacted surfaces revealed that, plastic deformation of the ductile matrix was the dominant erosion mechanism and the carbides fracture was negligible which led to small erosion rate. Whereas, at high impact angles (greater than 45^o) gross fracture and cracking of the carbides were the main erosion mechanisms in addition to indentation with extruded lips of the ductile matrix.

Many researchers [13–18] have been working on the erosion process modeling using different modeling techniques. In the early stages of the modeling of the erosion process, Finnie developed mathematical model mechanisms for ductile metals and solid surfaces [14] for a single particle impingement; Bitter [15-16] developed erosion models based on plastic deformation, cutting, Hertzian contact theory and energy balance equation approaches; Hutchings [17] developed a theoretical model based on a plastic strain approach for metals by exposure to spherical particles at normal impingement; and Hashish [18] modified Finnie's models to include the effect of the particle shape. Gee et al. [19] used a stepwise testing method for determining the mechanism of gas borne particulate erosion. Stepwise testing is an approach that has been recently developed as a way of providing information on the build-up of damage in erosion. The essence of the method is to incrementally expose a sample to erosion from small quantities of erodent and then be able to accurately relocate the test sample in the scanning electron microscope to enable the same area to be examined at high magnification, allowing for the development in damage to be followed up at specific points on the sample surface.

In the present work, the stepwise erosion combined with relocation scanning electron microscopy was used to follow up the real erosion processes with impact

angle in considerable detail. Based upon the SEM images, the size and the shape factor of the impact sites were analyzed. As well as the material removal processes were investigated.

2. EXPERIMENTAL DETAILS

Slurry erosion tests were carried out using a slurry whirling arm rig, which is schematically shown in Fig. 1. The test rig consists of three main units: a specimen rotation unit, a slurry unit and a vacuum unit. Full description of this rig and how it works as well as its dynamics are found in Ref. [12, 20-21]. The specimen rotation unit provides impact velocity. Two specimens of (23 x10 x 10 mm) are clamped to two specimen holders. During slurry erosion tests only the upper surface of specimen is exposed to the impinging slurry since the sides of the specimen are held by the specimen holder. The specimen holders have tilting and locking facilities to adjust the required inclination of the test specimen. As well as, the position of the sample was carefully marked so that the sample could be replaced in the same position in the erosion system. The impact angle can be adjusted to any required value by rotating the specimen holder around its horizontal axis, as shown in Fig. 2. The holders are mounted on the ends of the two arms of the rotator, which is driven by a variable speed

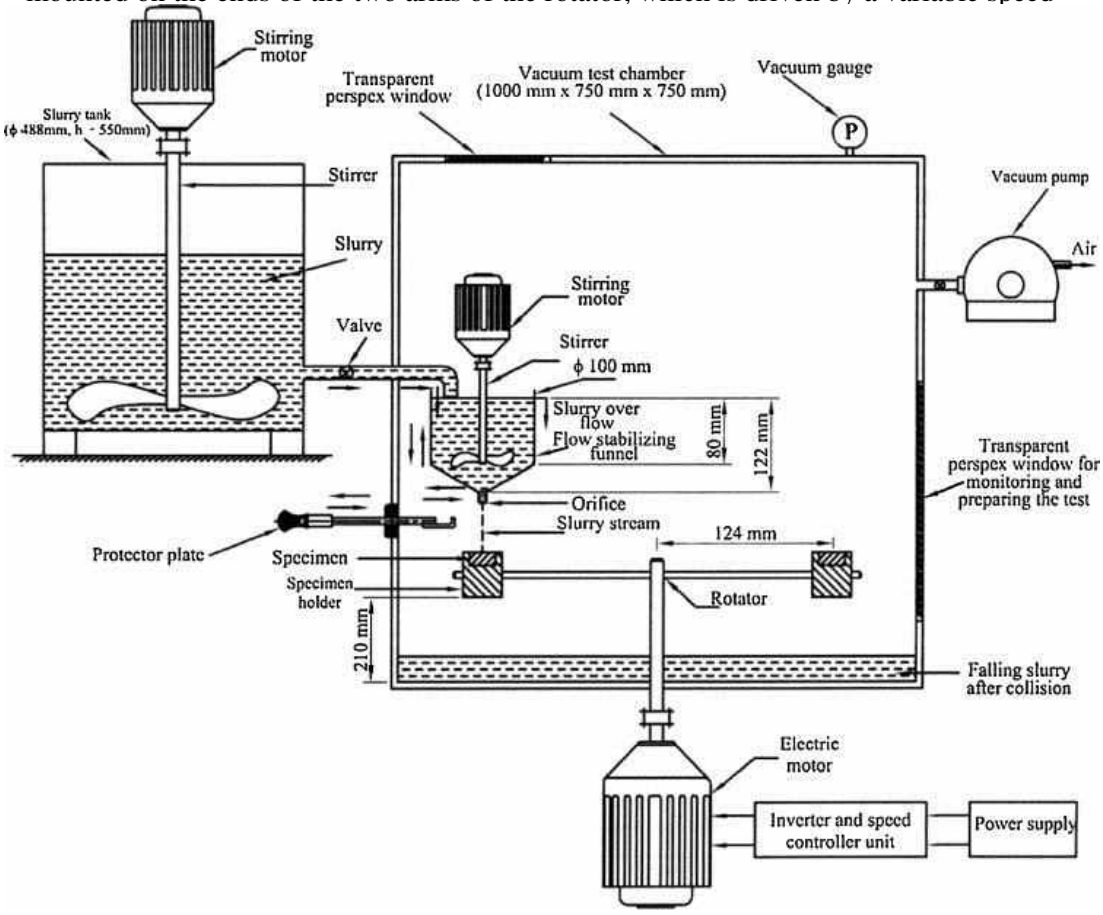

Fig. 1 Schematic diagram of the slurry erosion whirling –arm rig

The slurry whirling arm rig used in this work provides a homogenous stable slurry stream (a mixture of tap water and SiO_2). The velocity of falling slurry stream from the 3 mm diameter funnel orifice is 1.62 m/s, at the specimen surface, impacting every specimen at any pre-set angle between 0 deg. and 90 deg. The impact angle (θ) and impact velocity (v) are correlated to ensure the intended value, which can be obtained from the velocity vector diagram of particle impact, as shown in Fig. 2. The distance between the funnel orifice and the specimen surface is 40 mm. The slurry test chamber is evacuated by a vacuum system (up to 28 cm Hg) to eliminate aerodynamic effects on slurry system.

The test specimens were made from a commercial grade of alloy steel, namely AISI 5117. This type of alloy steel is used because it provides good machinability. The chemical composition and mechanical properties of the specimen material are listed in Tables 1 and 2, respectively.

Table 1: Chemical composition of low alloy steel AISI 5117.

Element	C	Si	Cr	Mn	S	P	Fe
Wt. %	0.17	0.3	0.9	1.2	0.003	0.005	Balance

Table 2: Mechanical properties of low alloy steel AISI 5117[22].

Yield Strength(MPa)	Tensile Strength (MPa)	Modulus of Elasticity (GPa)	Hardness, Hv (200g)	Density (Kg/m^3)
600	950	210	200	7850

To achieve identical initial condition for each test, the specimen's working faces were polished with SiC paper successively down to #4000. The resulting average surface roughness, R_a was 0.03 µm. Specimens were cleaned with acetone and dried with air blower before and after each test. Mass loss of the wear specimens was measured by an electronic balance of 100 g ± 0.1 mg.

Natural silica sand sieved to a nominal size range of 250 – 355 µm was used as an erodent. A scanning electron microscopy (SEM) photograph of typical sand particles is shown in Fig. 3. These particles were characterized [23] using an image analysis method in terms of the aspect ratio (W/L) and roundness factor ($P^2/4\pi A$), where W is the particle width, L is the particle length, A is the projected area of the particle and P is its parameter. The statistical values of the particle parameters are given in Table 3.

Table 3: Statistical values of particle size and shape as obtained by image analysis of SiO_2 particles

Particle size range(µm)	Statistical parameters	Area (μm^2)	Average diameter (µm)	Length, L(µm)	Width, W(µm)	Aspect Ratio, W/L	Perimeter, P(µm)	$P^2/(4\pi A)$
250-355	Mean	76336.88	301.10	387.08	272.76	0.7180	1117.48	1.36
	Median	76040.1	300.99	375.81	276.32	0.736	1108.79	1.25
	Standard deviation	20,507.5	43.60	64.29	44.68	0.14	161.34	0.38

Since the properties of solid particles (i.e., shape, hardness …etc.) are of great importance, a single source of erodent particles was used throughout the experiments. Also, fresh particles were used in each test to avoid any degradation of impacting particles during erosion tests. In these series of tests, the particles concentration was held at 1 wt% and the impact velocity of slurry stream was 15 m/s.

The difference between the apparatus used in the present study (slurry whirling arm rig) and the other apparatus used in this field of study is the absence of dependence on time in the present apparatus regarding the comparison among the different impact angles. As shown in Fig. 2, the amount of particles which impacts the surface of specimen differs from one angle to another. Consequently, comparison of the mass loss with the impact angle curves at the same test-time will give misleading results. Therefore, in studying the effect of impact angle on slurry erosion processes the tests will be performed at the same amount of particles impacts the specimens at different impact angles. The amount of particles which impact the surface of specimen as a function of the impact angle is derived from the geometry of the impacting process, as shown in Fig. 2 [12].

The mass of particles striking each specimen per revolution is given by;

$$m_p = \left[l \sin(\theta_o) A_n + \frac{l Cos(\theta_o)\, Q}{\pi D N} \right] C_w \rho_w \qquad (1)$$

Where,

θo: the angle between the surface plane of the specimen and the horizontal plane

l: is the length of wear specimen surface in m

A_n: is the area of orifice in m^2

C_w: is the weight fraction of solid particles in the water

ρ_w: is the water density in kg / m^3

D: is the rotational diameter of the wear specimen in m

Q: is the volume flow rate of slurry in m^3/min. and

N: is the rotational speed of the wear specimen in rpm.

To implement the stepwise erosion approach the specimens were exposed to aliquots of erodent. Preliminary tests showed that the suitable size of aliquot was 1.3 gm since it was able to make visible and isolated individual impact events at different impact angles. The tests were carried out for 4 aliquots and at impact angles of 30 °, 45 °, 60 ° and 90 °. At the starting of experiment, the specimen was exposed to the first aliquot of erodent. It was then taken from the test rig, cleaned as described earlier and examined in SEM. After the appropriate images had been taken, the specimen was exposed to further aliquot of erodent.

The relocation scanning electron microscopy depends on marking the specimen so that the same area on the specimen could be found repeatedly. For examining the eroded surface morphology features, SEM photographs with high magnification were taken. For quantitative morphological analysis of impact sites, such as number, size, perimeter.. etc, a low magnification were used.

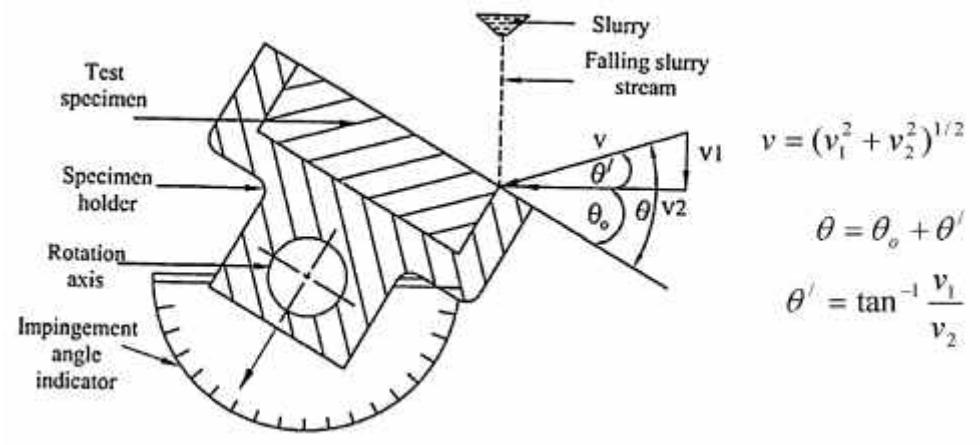

Fig. 2 Schematic diagram of impact velocity and impact angle.

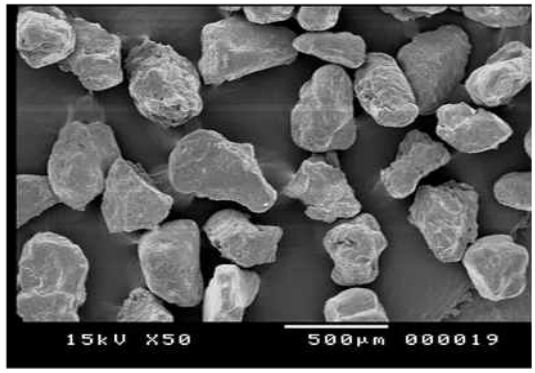

Fig. 3 Scanning electron microphotograph of silica sand (mean diameter = 302µm).

3. RESULTS AND DISCUSSION

3.1 Impact Craters

3.1.1 Number of Impact craters.

At first, three positions were identified on the eroded specimen surfaces, two at the leading and trailing edges and the third near the midway of the specimen. Then the aspects of the affected area characteristics, i.e. the number, shape and size of erosion sites are systematically investigated for successive stages and different impact angles. It is to be noted in this work, that all impact sites developed on eroded surface we called them craters. The counting process was carried out on a large digital screen to facilitate the counting process. The counting process was very exhausting process, in determining whether this crater occurred because of one particle or more. In this process, some uncertainty associated with the number of impacts might be found. However, this uncertainty will be very small because of the small exposure. Due to small exposure, the number of impacts was few and to some extent the impact sites

were isolated and clear. The number of impacts was counted manually for each specimen at three positions mentioned above and then the average was calculated.

Figure 4 presents a series of relocated area that resulted from the stepwise erosion tests on the AISI 5117 steel for impact angles of 30^o, 45^o, 60^o and 90^o. The white areas in these photos represent the impact craters. The inclined vertical lines are the traces of polishing lines. The counted number of craters is plotted versus the mass of erodent for different impact angles as shown in Fig. 5. It can be observed that the number of craters increases almost linear with the increase in the mass of erodent for all tested angles. It can also be observed that the number of craters decreases with the increase of angle. In order to see whether these data correspond with the results of loss in mass of the sample against the erodent mass, cumulative mass loss of steel 5117 versus mass of erodent at different impact angles was obtain experimentally and presented graphically in Fig. 6. Curves in Fig. 6 have the same trend as those in Fig. 5. Moreover, from Fig. 6, it is obvious that the mass loss due to erosion increases with the increase of impact angle from 30^o up to 45^o where it reaches its maximum value. Further increase of the impact angle beyond 45^o up to 90^o leads to continuous decrease in mass loss. It reaches its minimum value at normal impact. This represents a typical behaviour of ductile material subjected to slurry erosion .To understand the dynamics of particles, i.e. the efficiency of impact, rebound effect, particle irregularity …etc, the number of craters is compared with the number of particles presumably impacting the specimen surface during each stage. By assuming the efficiency of impact 100%, the number of impact particles can be found by knowing the mass of erodent which impacts the surface of specimen at each exposure and for each impact angle. Since it is verified that this test rig [12] provides a homogeneous mixture, the particles will be uniformly distributed on the eroded area. In this study, all microphotographs have the same size for each exposure, also for all impact angles, all microphotographs have the same magnification. So, knowing the factor of magnification and the size of studied microphotographs in relation to the whole eroded area, the calculated number of particles which impacts the selected microphotographs can be estimated. For comparison between the counted number of craters and the number of particles, the later is shown plotted in Fig. 5. From Fig. 5, one can observe that the counted number of crater is larger than the calculated number of particles for all impact angles and at any stage.

The pertinent factors that can lead to the increase in the number of crater more than the number of calculated impact particles may be the rebound effect of particles, the irregular shape for these particles and particle fragmentation. When the particles strike the substrate, part of their kinetic energy is spent on removing the material, part on indentation of substrate, and a part on rebounding. Stack et al. [24] in their study on the effect of elastic rebounds reported that at velocities that might typically be encountered with slurry pipe lines, for instance between 1 ms^{-1} and 10 ms^{-1}, the coefficient of restitution is significant. This may lead to the conclusion that the effect of the rebound of the particle, and the elastic forces often deemed negligible, cannot in fact be ignored. By using the whirling arm test rig, Abouel-Kasem et al. [20] in their study on the effect of the rebound particles reported that most experimental works for slurry used a slurry jet where the rebound particles have a negative effect in developing erosion, since the erodent particles rebounded from the sample surface shield the

surface by their collision with incident particles. For the whirling arm test rig, the effect of the rebound particles cannot be neglected. In this tester, no shielding of surface occurs as it occurs in the slurry jet. Particle fragmentation leading to secondary erosion has been observed by Tilly [25] in his work using quartz on H46 steel. It was assumed that the amount of fragmentation and secondary erosion would be dependent of the particle velocity, size, impact angle and difference in hardness between the erodent and target surface.

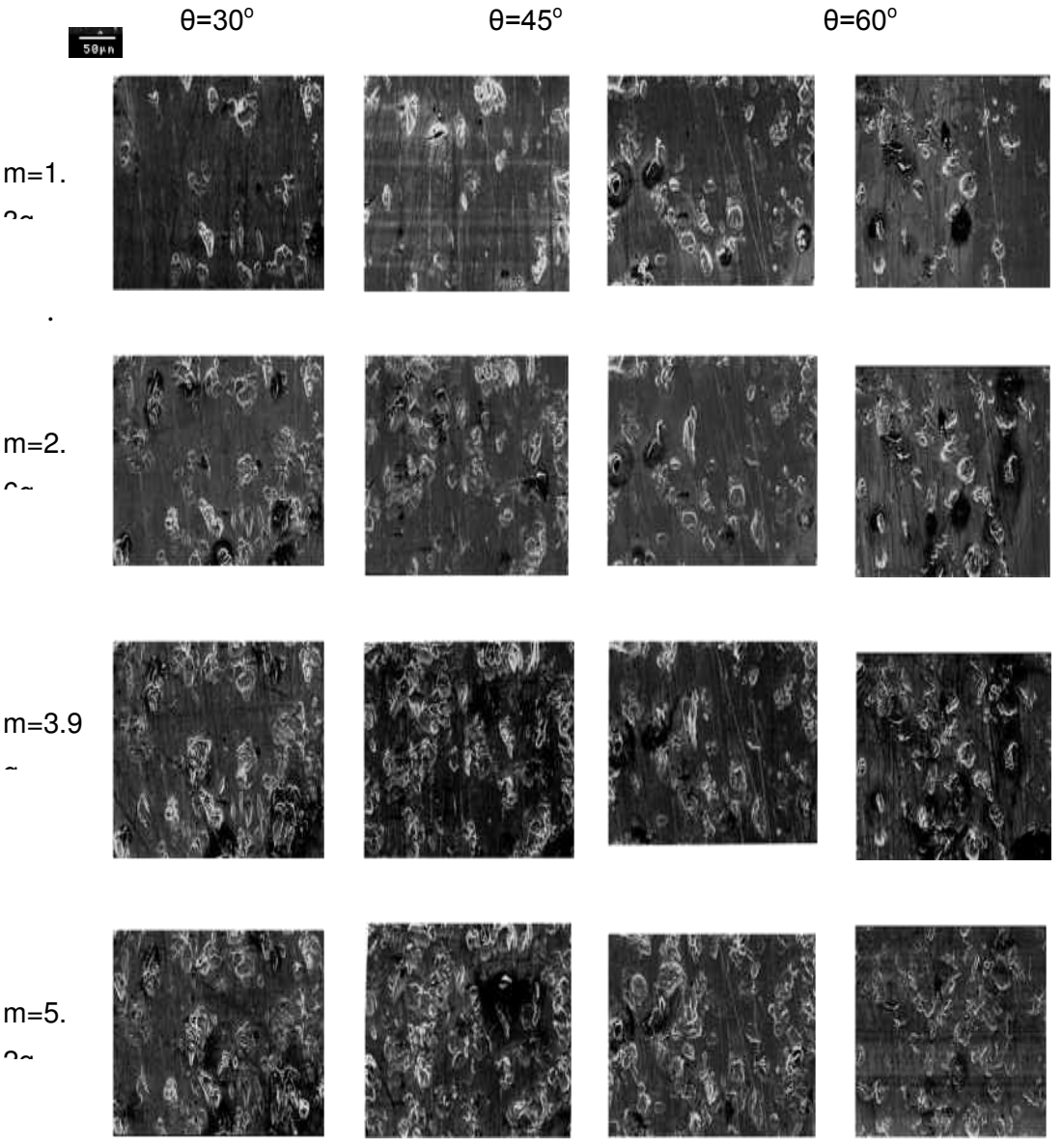

Fig. 4 Scanning electron microphotographs of 5117 alloy steel eroded surfaces at different impact angles and mass of erodent during the four successive stages.

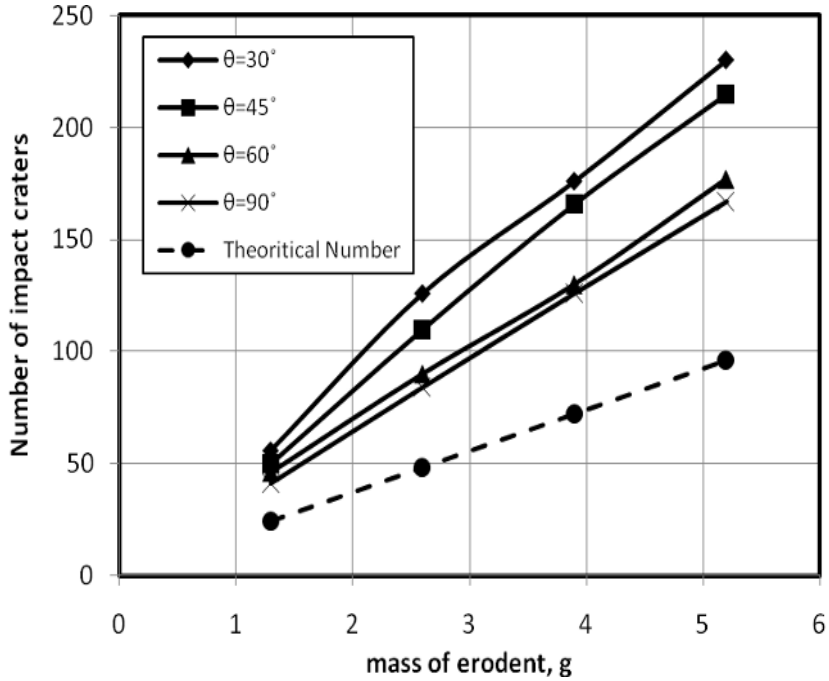

Fig. 5 Number of accumulative impact craters versus mass of erodent for different impact angles.

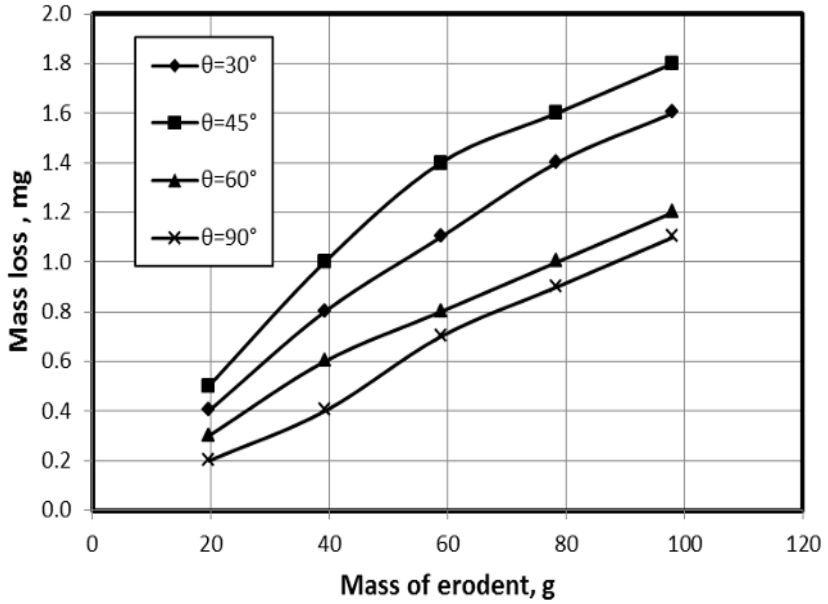

Fig. 6 Cumulative mass loss of low alloy steel 5117 versus mass of erodent for different impact angles.

3.1.2 Impact crater morphology

The damage developed on the carbon steel specimen surfaces at different impact angles and a mass of erodent of 2.6g is shown in Fig.7. It can be generally observed that the impact craters formed at angles of 15^o, 30^o, 45^o and 60^o have tracks in the direction of slurry stream, which is from bottom to the up of the micrographs. While for angles of 75^o and 90^o, it is hard to distinguish such directionality of slurry. However , closer observation for the micrographs at 75^o and 90^o, it can be seen that some craters have a random directionality as shown by arrows in Fig. 7(e and f).This may be attributed to the divergence of particles. Therefore, the effect of impact angle based on the impact crater shape, which developed here for a ductile material, can be divided into two regions; the first region for $\theta \leq 60^o$ and the second region for $\theta \geq 75^o$. In the first region the length of the tracks decreases with the increase of impact angle Fig. 7(a-c). On the other hand, from these micrographs depicted in Fig. 7, it can be inferred that the actual impact angle of particles differed from the nominal one. This can be observed from the relative position of the impact craters to each other. This observation had been noted in the literature based on fluid flow analysis [26].

The development of crater size with the mass of erodent and impact angle is shown in Fig.8. The crater size range was the least for the normal impact and was from few micrometers to about 50 μm. For angles of 30^o and 60^o, the upper limit of the range exceeds than that for normal impact and reached 100 μm. The crater size range for the angle of 45^o was similar to that for angles of 30^o and 60^o, except the lower limit of the range shifted to a higher value of two digits. Generally, by comparing the lower and upper limit crater size range with the average size of particle of 302 μm, they represent about 3 % and 30%, respectively. This means that the impact process of particles depends on the orientation and angularity of particles. For the small crater sizes, it may be produced by one of the particle protrusions. While the large one it may be formed by the body of particles (labeled A) or by more than one protrusion (labeled B) as shown in Fig. 7(a).

3.2 Tracking the effects of removal of materials

Figures 9-11 show the sequence of images of damage developed after exposure to aliquots of erodent at impact angles of 45^o, 60^o and 90^o, respectively. On the first exposure, considerable damage to the surface occurred. This damage depends on the mechanisms related to the impact angle. The microcutting and ploughing were the dominant mechanisms for acute angle, while indentations and material extrusion prevailed for the normal impact [12]. The examination of slurry erosion behavior of subsequent stages shown in Figs. 9-11(b, c and d) reveals that the particle impact processes include the following events; forming new impact sites, impacting former sites, impacting the surface but without noticeable effect. The new impact sites that are formed in the subsequent stages, after stage no. 1 are encircled as shown in micrographs. When new particles impact former impact sites, the chips and the extruded materials formed at low and high impact angle, respectively, in the impact sites will be detached. Under subsequent impacts for these sites, it was observed that in some of the impact sites craters were formed and the others disappeared. From Fig. 11, it is noteworthy that the sequence of images illustrating the development of damage at

normal impact shows increase in the number of craters (impact sites) without noticeable detachment of the extruded metal. This explains the well known fact that the mass loss due to slurry erosion is minimum at normal impact angle.

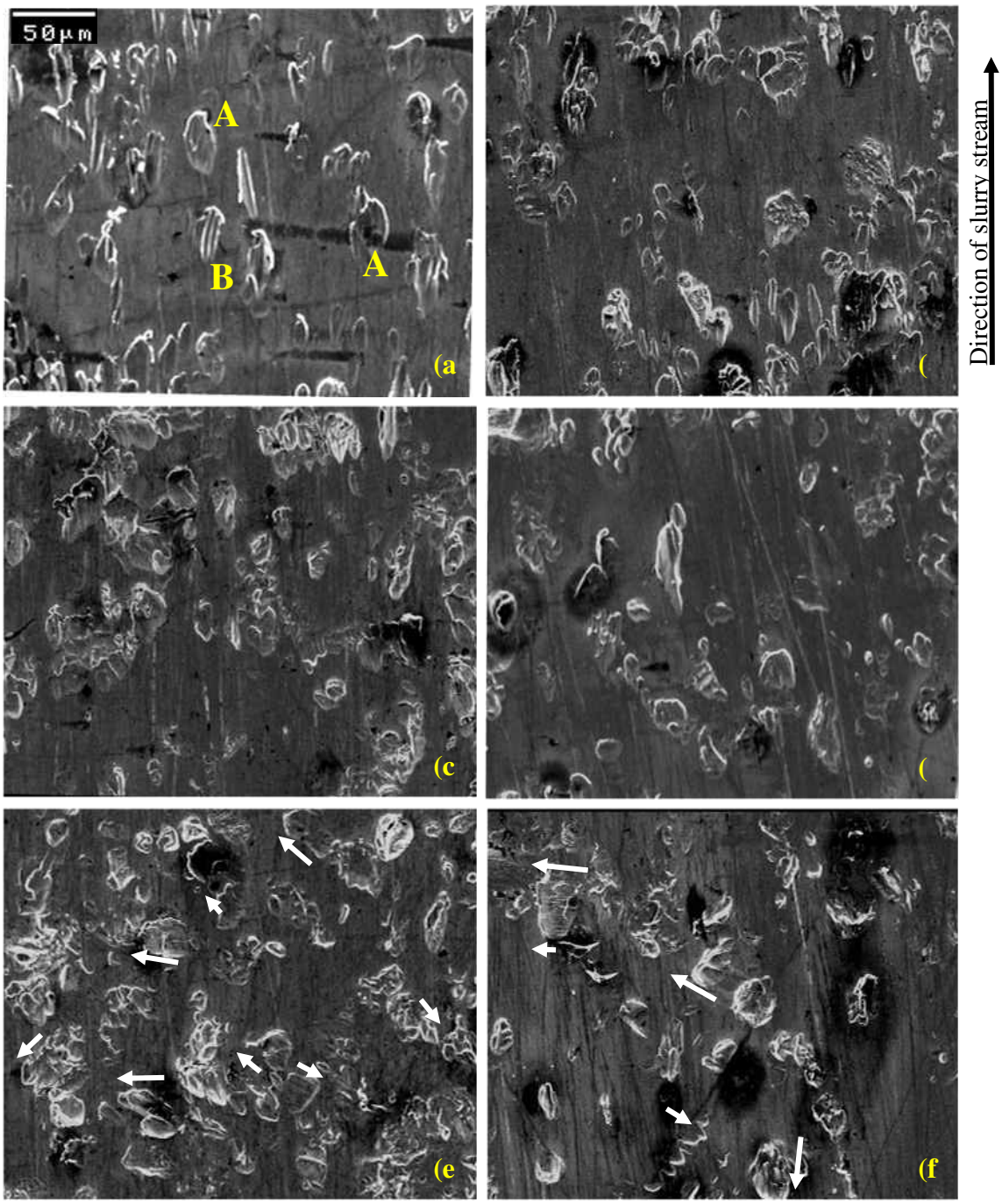

Fig.7 Damage on the carbon steel specimen surfaces at mass of erodent of 2.6 g and different impact angles: a-15°, b- 30°, c-45°, d-60°, e-75° and f- 90°

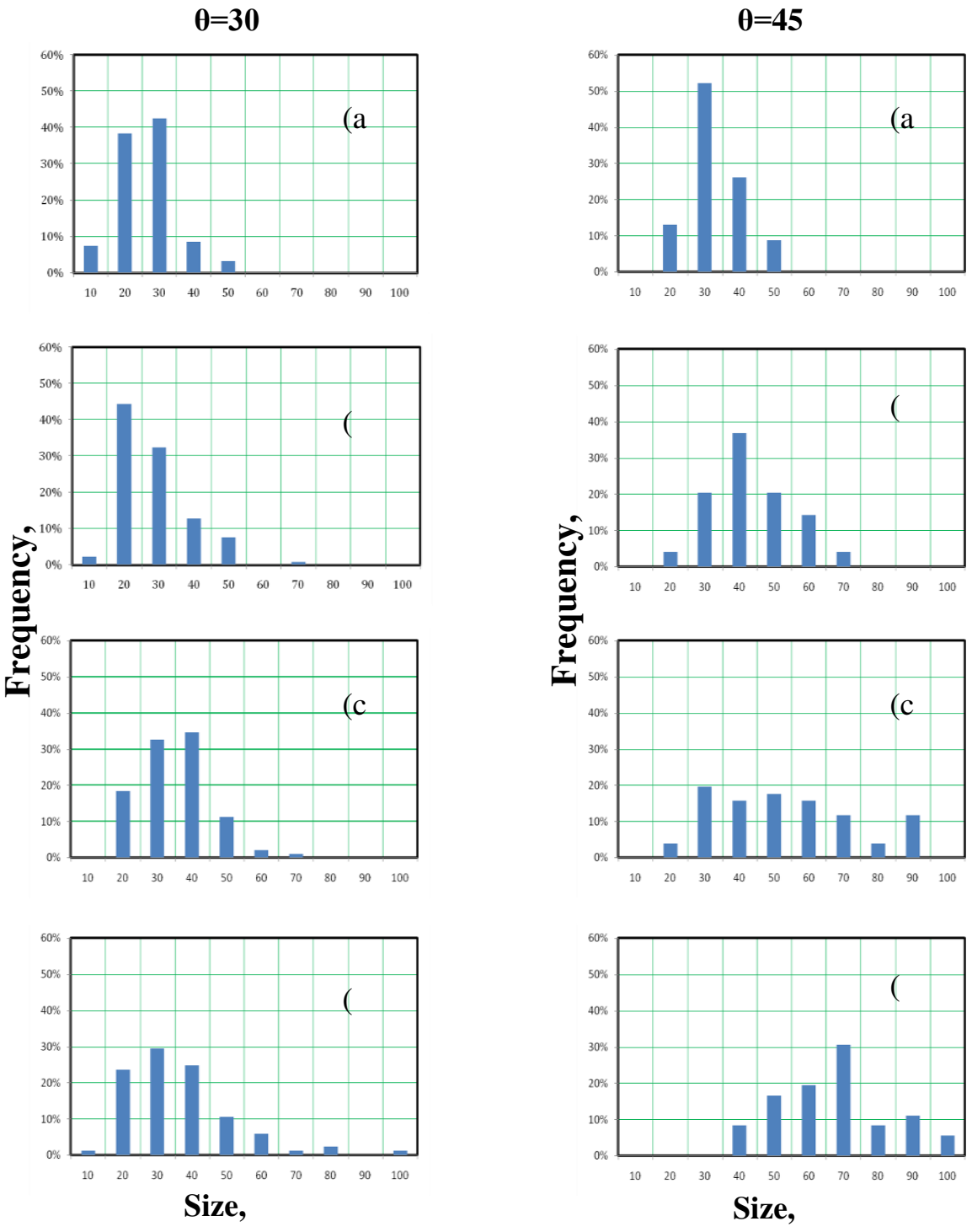

Fig. 8 Crater size distributions with different impact angles and after exposure of (a) 1.3g, (b) 2.6 g, (c) 3.9 g, (d) 5.2 g

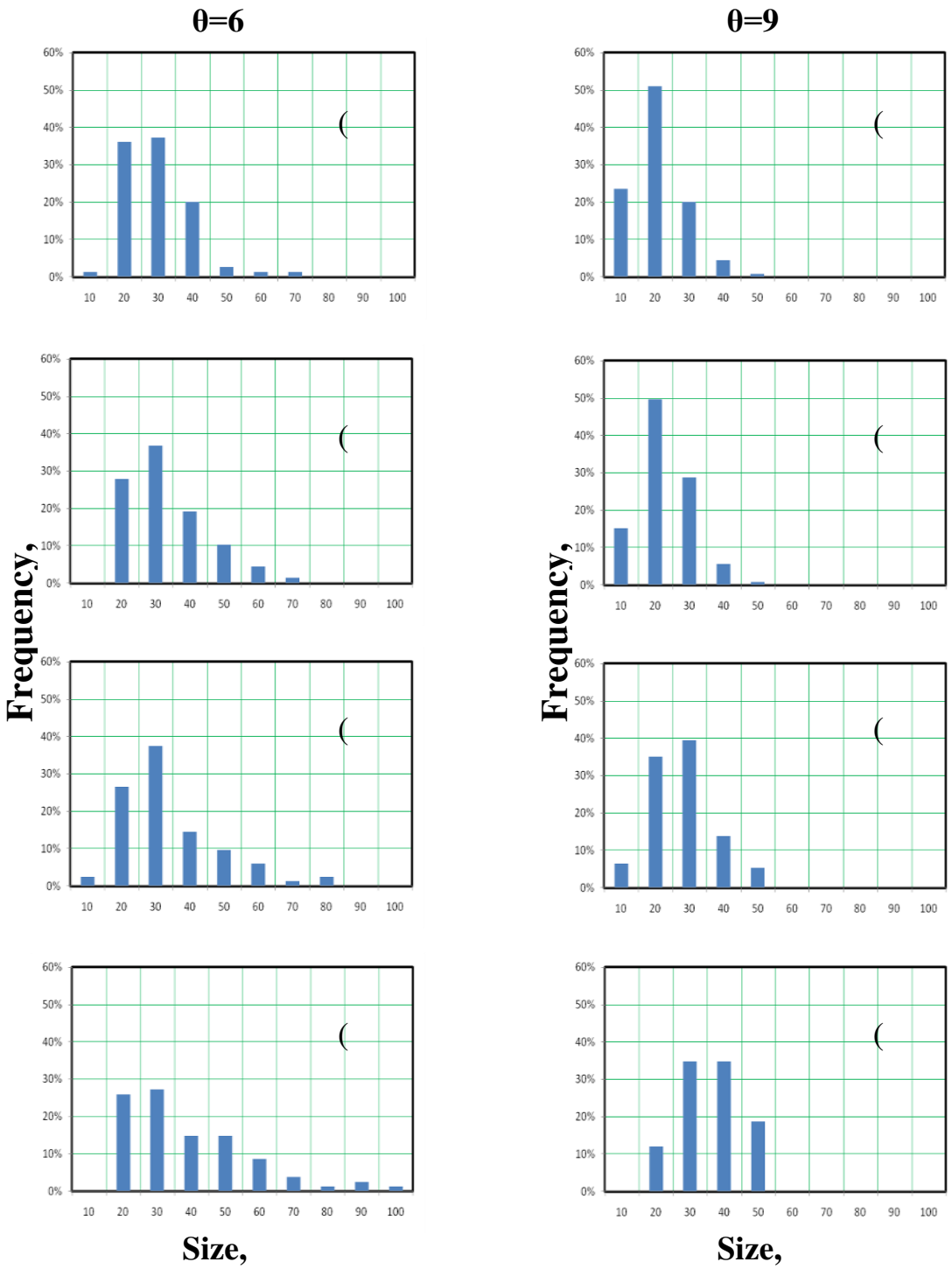

Fig. 8 (continued)

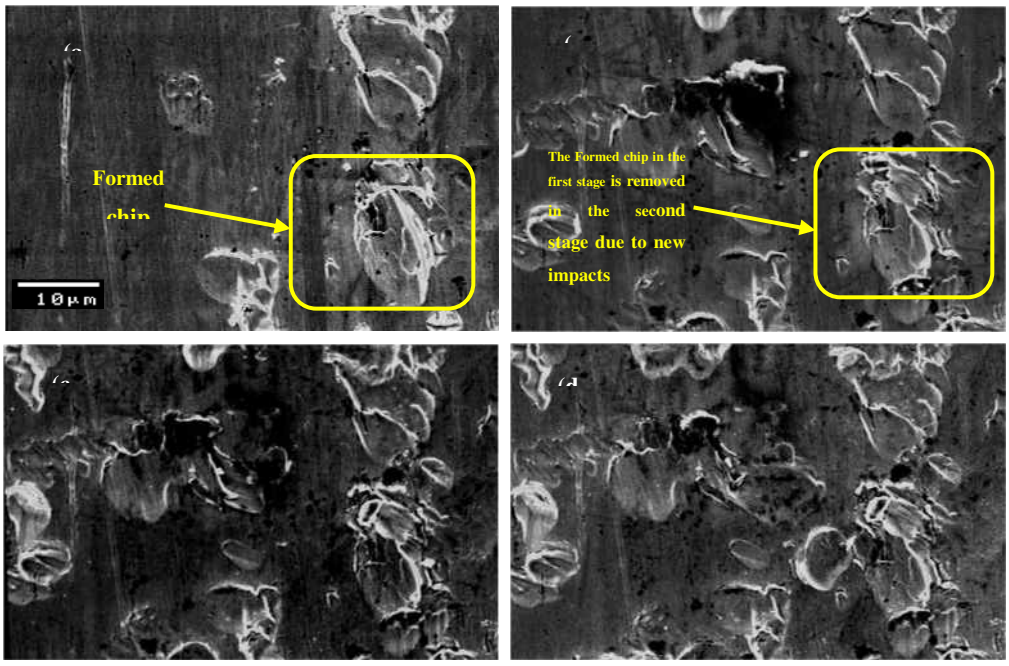

Fig. 9 Sequence of images illustrating development of damage at the impact angle of 45° after exposure to (a) 1.3g, (b) 2.6 g, (c) 3.9 g, (d) 5.2

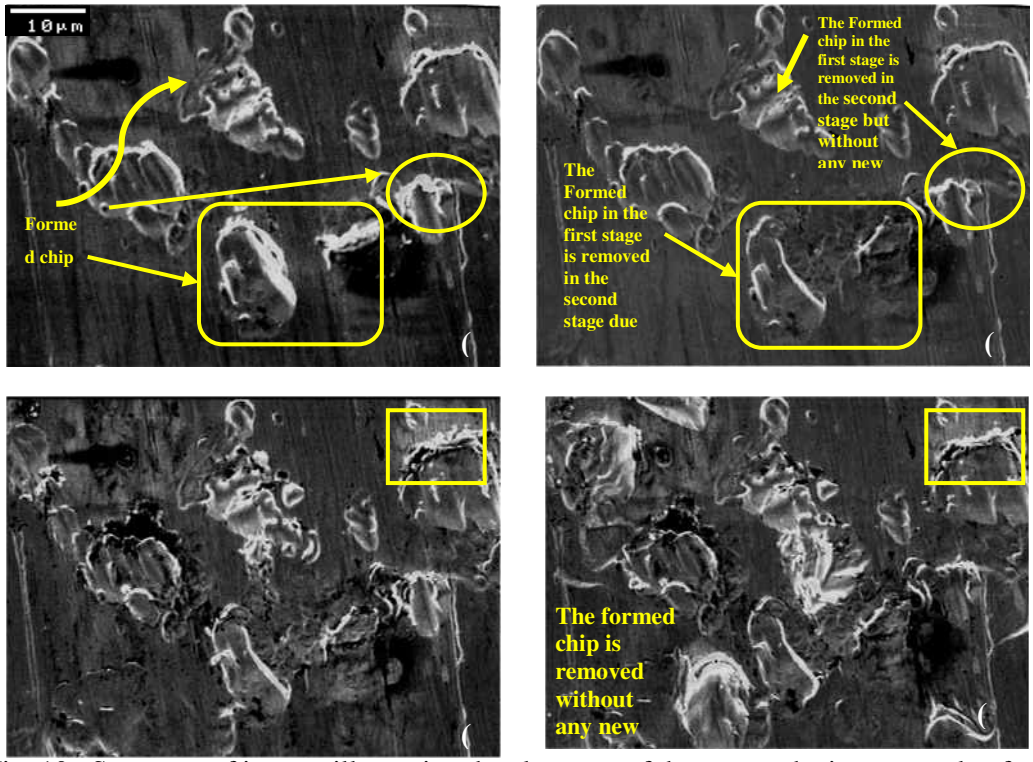

Fig. 10 Sequence of images illustrating development of damage at the impact angle of 60° after exposure to (a) 1.3g, (b) 2.6 g, (c) 3.9 g, (d) 5.2 g.

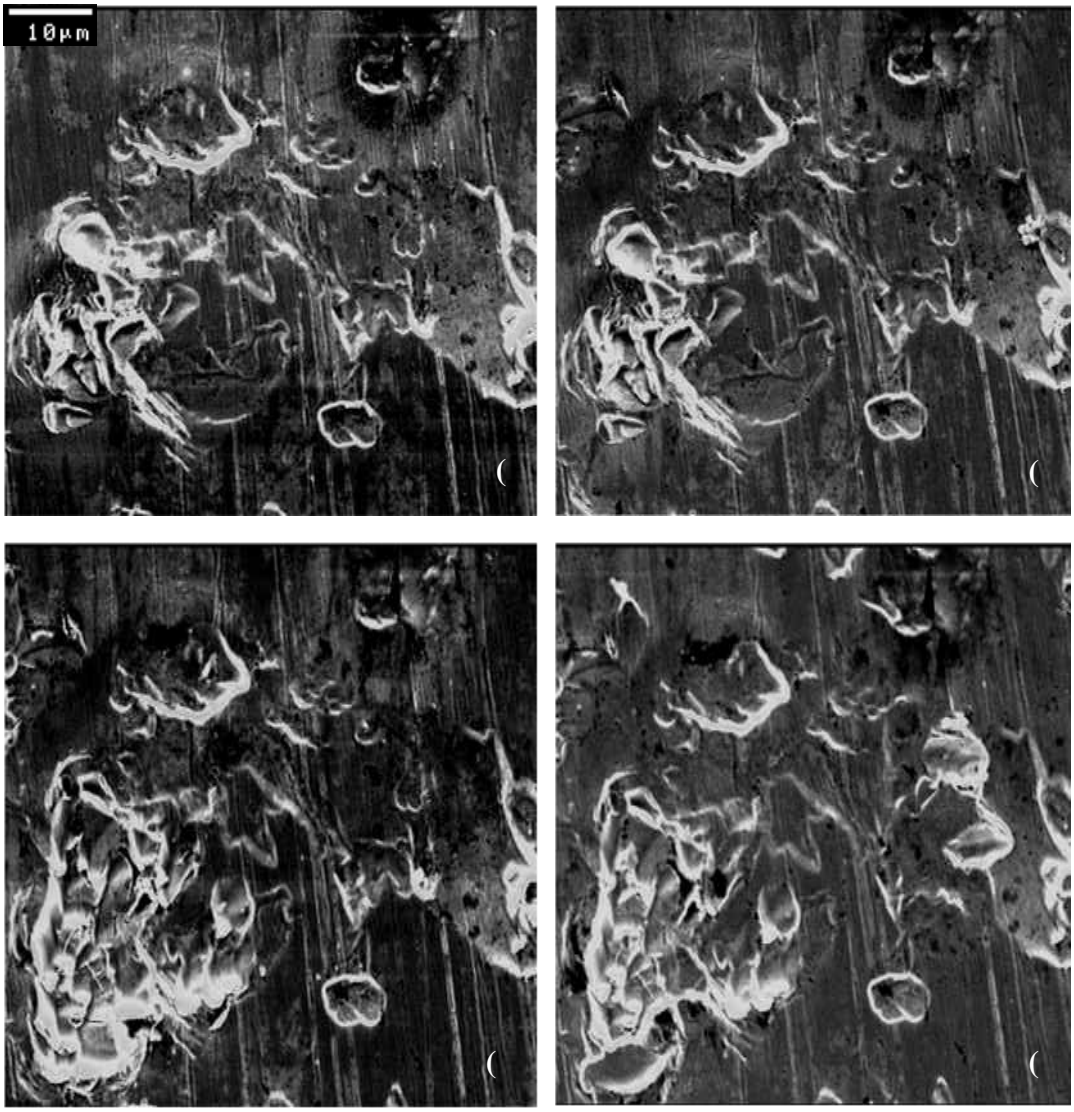

Fig. 11 Sequence of images illustrating development of damage at the impact angle of 90^{o} after exposure to (a) 1.3g, (b) 2.6 g, (c) 3.9 g, (d) 5.2 g.

4 CONCLUSIONS

1. The impact sites or craters are counted using stepwise erosion. It was found that the number of craters increases with the increase of erodent for all impact angle. As well as, the number decreases with the increase of impact angle.
2. Based upon analysis, the results showed that the number of craters is larger than the calculated number of particles of erodent. This is interpreted in the light of rebound and particle fragmentation.

3. Using image analysis for stepwise eroded surface, the crater size was characterized into two regions according to the impact angle. The first region for $\theta \leq 60^{o}$ and the second region for $\theta \geq 75^{o}$. In the first region, the crater size range was from few micrometers to about 100 µm. However, in the second region the upper limit of crater size rang was the least and it was about 50 µm. The results showed also that the lower limit of the size range for the angle of 45^{o} rose to two digits.
4. The material removal by chipping as result of subsequent particle impacts plays an important role in slurry erosion process.

REFERENCES

[1] Fang, O., Sidky, P.S., and Hocking, M.G., "Microripple Formation and Removal Mechanism of Ceramic Materials by Solid-Liquid Slurry Erosion" Wear, **223**, pp. 93-101, (1998)**.**

[2] Lathabai, S., and Pender, D. C.,"Microstructure Influence in Slurry Erosion of Ceramics" Wear, **189**, pp.122-135, (1995).

[3] Li, Y., Burstein, G.T., and Hutchings, I. M., "The Influence of Corrosion on the Erosion of Aluminum by Aqueous Silica Slurries", Wear, **186-187**, pp. 515-522, (1995).

[4] Iwai, Y., and Nambu, K.,"Slurry Wear Properties of Pump Lining Materials" Wear, **210**, pp. 211-219, (1997).

[5] Tsai, W., Humphrey, J.A.C.,Cornet, I.,and Levy,A.V., "Experimental Measurement of Accelerated Erosion in a Slurry Pot Tester" Wear, **68**, pp. 289-303, (1981).

[6] Stanisa, B., and Ivusic, V.,"Erosion Behaviour and Mechanisms for Steam Turbine Rotor Blades", Wear, **186-187**, pp. 395-400, (1995).

[7] G.T. Burstein and K. Sasaki," Effect of Impact Angle on the Slurry Erosion–Corrosion of 304L stainless steel", Wear **240**, pp. 80–94, (2000).

[8] Y.I. Oka, H. Ohnogi, T. Hosokawa and M. Matsumura, "The Impact Angle Dependence of Erosion Damage Caused by Solid Particle Impact", *Wear* **203–204**, pp. 573–579, (1997).

[9] H.M. Clark and K.K. Wong, "Impact Angle, Particle Energy and Mass loss in Erosion by Dilute Slurries", *Wear* **186–187**, pp. 454–464, (1995).

[10] Q. Fang, H. Xu, P.S. Sidky and M.G. Hocking, " Erosion of Ceramics Materials by a Sand/Water Slurry Jet", *Wear* **224**, pp. 183–193, (1999).

[11] K.C. Chen, J.L. He, W.H. Huang and T.T. Yeh," Study on the Solid–Liquid Erosion Resistance of Ion-Nitrided Metal", *Wear* **252**, pp. 580–585, (2002).

[12] Al-bukhaiti, M.A., Ahmed,S.M., Badran, F.M.F., Emara, K. M., "Effect of Impact Angle on Slurry Erosion Behavior and Mechanisms of 1017 Steel and High-Chromium White Cast Iron",Wear,**262**,pp.1187-1198, (2007).

[13] Finnie, I.," The mechanism of erosion of ductile metals", Proceedings of the Third National Congress on Applied Mechanics, New York, pp. 527–532, (1958).

[14] Finnie, I.," Erosion of surfaces by solid particles", Wear **3**, 87–103, (1960).

[15] Bitter, J.," A study of erosion phenomena, part 1", Wear **6**, 5–21, (1963).

[16] Bitter, J.," A study of erosion phenomena, part 2" Wear **8**, 161–190, (1963).
[17] Hutchings, I.M., "A model for the erosion of metals by spherical particles at normal incidence", Wear **70**, 269–281, (1981).
[18] Hashish, M.," An improved model of erosion by solid particle impact", 7th International Conference on Erosion by Liquid and Solid Impact, Cambridge, pp. 461–480, (1987).
[19] Gee,M.G., Gee, R. H., McNaught, I.,"Stepwise erosion as a method for determining the mechanisms of wear in gas borne particulate erosion", Wear, **255**, pp. 44–55, (2003).
[20] Abouel-kasem, A., Abd-Elrhman,Y.M., Ahmed,S.M. and Emara,K.M.,"Design and Performance of Slurry Erosion Tester", ASME J.Tribol.,132(2), pp. 021601, (2010).
[21] Abouel-kasem, Al-Bukhaiti,M.A., Ahmed, S.M. and Emara,K.M., "Fractal Characterization of Slurry Eroded Surfaces at Different Impact Angles",Tribology,ASME,131, pp. 1-9, (2009).
[22] Bohler," Special Steel Manual", A-8605 Kapfenberg, Germany, pp. 90–98, (2000).
[23] Abouelkasem, A. ," Particle Size Effects on Slurry Erosion of 5117 steels", ASME J.Tribol.,133, pp. 014502-1, (2011).
[24] Stack, M.M., Corlett, N., and zhou, S., "Some Thoughts on Effect of Elastic Rebounds on the Boundaries of the Aqueous Erosion – Corrosion", Wear, 214, pp. 175-185, (1998).
[25] H.C. Clark, " The Influence of flow field in slurry erosion", *Wear* 152, pp. 223-240, (1992).
[26] Tilly, G.P.,"A Two Stage Mechanism of Ductile Erosion," Wear 23, pp. 87-96, (1973).

التآكل التدريجي كطريقة لدراسة اليات التاكل عند زوايا التصادم المختلفة فى التاكل بالنحر

فى هذا المبحث تم استخدام منهجالتآكل التدريجى لنفس الموقع لدراسة تأثير زاوية التصادم على عملية التاكل لصلب الفولاذ (AISI 5117) بصورة مفصلة. تم دراسة وفحص عدد مواقع الصدماتوطرق تشكلها عند زوايا التصادم المختلفة باستخدام مجهر الماسح الإلكتروني ثم تحليل الصور المجهرية. بالاضافة الى ذلك الصور المجهرية للسطح المتآكل باستخدام المنهج التدريجي لنفس الموقع تم التقاطها وتحليلها للوصول إلى الفهم الجيد لآلية الفقد فى المادة عند زوايا التصادم المختلفة. تم اجراء اختبارات التاكل عندما كان تركيز الحبيبات الصلبة 1%, وسرعة التصادم للسائل المتدفق المحمل بالحبيبات الصلبة 15 م/ث. حجم حبات سيليكا الرمل المستخدمة فى اختبارات التاكل على جهاز التآكل ذو الذراع الدوار من 250 – 355 مم. بينت النتائج ان عدد الخبطات يزداد كما هو متوقع مع زيادة كمية الحبيبات الصادمة لكل زوايا التصادم وهذا العدد يقل مع زيادة زاوية التصادم. كما ان عدد الخبطات التى تم حصرها اكبر من عدد الخبطات المحسوبة نظريا عند كل الزوايا وعند كل المراحل. تاثير زاوية التصادم بالاعتماد على شكل الخبطة يمكن ان يقسم الى منطقتين؛ المنطقة الاولى عندما تكون $\theta \leq 60°$ والمنطقة الثانية عندما تكون $\theta \leq 75°$. فى المنطقة الاولى طول المسار يقل مع زيادة زاوية التصادم. فى المنطقة الاولى حجم الخبطات يتراوح من ميكرومترات قليلة الى 100 مم والى 50 مم فى المنطقة الثانية. الرايش المتكون نتيجة تتابع تصادم الحبيبات يلعب دورا مهما فى تطور التاكل.

كلمات البحث: التاكل بالنحر, زاوية التصادم, عدد الخبطات, السطح المتآكل, آليات التآكل, صلب الفولاذ (AISI 5117), تأثير ارتداد الحبيبات.